Guanidinium Manipulated Interfacial Polymerization for Polyamide Nanofiltration Membranes with Ultra-high Permselectivity

Shuting Xu [a,b], Jiahuan Liu [a, c], Jianqiang Wang [a,b], Haibo Lin [a,b], Qiu Han [a,b], Fu Liu [a,b]*, Chuyang Y. Tang [d]*

[a] Zhejiang International Joint Laboratory of Advanced Membrane Materials & Processes, Ningbo Institute of Materials Technology & Engineering, Chinese Academy of Sciences, No. 1219 Zhongguan West Rd, Ningbo 315201, China

[b] Ningbo College of Materials Technology & Engineering, University of Chinese Academy of Sciences, 19 A Yuquan Rd, Shijingshan District, Beijing 100049, China

[c] School of Materials Science and Chemical Engineering, Ningbo University, No. 818 Fenghua Rd, Ningbo 315211, China

[d] Department of Civil Engineering, The University of Hong Kong, Pokfulam, Hong Kong 999077, China

* Corresponding author at:

Prof. Fu Liu, Ningbo Institute of Materials Technology & Engineering, Chinese Academy of Sciences, No. 1219 Zhongguan West Rd, Ningbo 315201, China, E-mail address: fu.liu@nimte.ac.cn

Prof. Chuyang Y. Tang, Department of Civil Engineering, The University of Hong Kong, Pokfulam, Hong Kong 999077, China, E-mail address: tangc@hku.hk

Graphical abstract

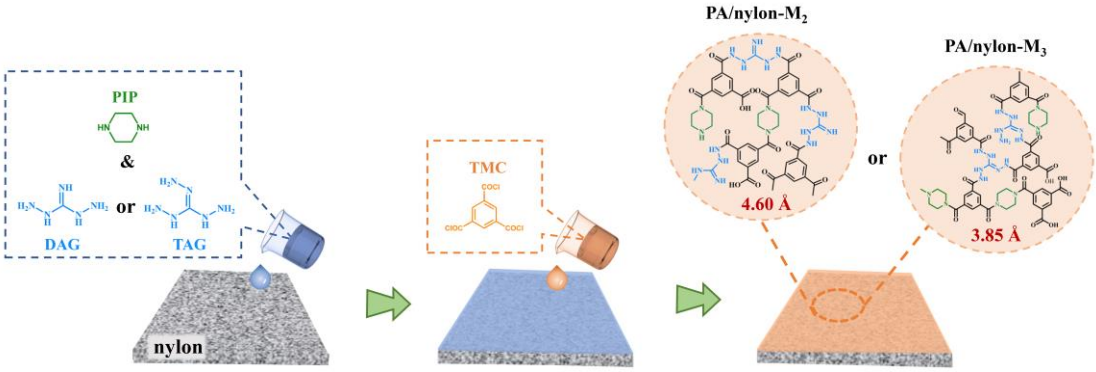

Abstract

Polyamide (PA) nanofiltration (NF) membranes with excellent permeability and selectivity have always been the ultimate pursuit of desalination technology. Herein, we present a guanidinium manipulated interfacial polymerization strategy to develop guanidyl-integrated PA NF membranes with ultra-high permselectivity. A nylon microfiltration membrane is utilized as the support to conduct spatial-temporal regulation of amine monomers along with controllable diffusion reaction. Through introducing 1,3-diaminoguanidine (DAG) or triaminoguanidine (TAG) into the aqueous piperazine solution, the free volumes of PA membranes could be well modulated at the sub-angstrom scale. Consequently, the TAG-integrated PA membrane exhibited high water permeance of 33.1 LMH·bar^{-1} and superior Na_2SO_4 rejection of 99.2%. Meanwhile, this membrane achieved outstanding anion sieving capability (Cl^-/SO_4^{2-} ~ 343) and nearly 100% tetracycline removal, which is superior to the "state-of-the-art" PA NF membranes. The DAG-integrated PA membrane attained ultra-high water permeance of 46.5 LMH·bar^{-1} due to its relatively large free volume. In addition, the nylon composite PA membranes displayed desirable anti-pressure and organic solvent-resistant abilities. This study provides a convenient and scalable preparation strategy for highly permselective NF membranes, which holds great application potential in desalination and resource recovery.

Keywords: polyamide membrane, nanofiltration, guanidinium, free volume, permselectivity.

1. Introduction

One third to nearly half of global urban population may face water scarcity in 2050 [1, 2]. Nanofiltration (NF) is a green, clean, and efficient membrane separation technology, which could play an important role in desalination, water softening, and resource recovery [3, 4]. The polyamide (PA) selective layer with highly crosslinked structure and negatively charged surface is created by the fast and elusive interfacial polymerization (IP) between the amine monomers in aqueous phase and the acyl chloride monomers in oil phase [5, 6]. The PA layer is conductive to intercepting high-valent ions and micropollutants according to size exclusion and Donnan effect [7]. However, the inherent physicochemical properties of PA polymer face arduous challenges of simultaneously enhancing water permeance and ion selectivity due to the "trade-off" effect [8-11].

In order to break through the "trade-off" limitation, researchers constantly devote to optimizing IP diffusion kinetics to acquire thin and dense PA layers, showing critical concerns about the spatial-temporal regulation of aqueous monomers [12-16]. The interface polymerization of highly reactive amine and acyl chloride monomers is less controlled due to instantaneous reaction. Ideally, spatial uniform distribution of amine monomers is beneficial to interface crosslinking for satisfying selectivity [17]. In addition, temporal manipulation could retard amine monomers diffusion to acquire relatively thin film for high flux [18-21]. The surface micro-nano structure, pore size, porosity, wettability, affinity and surface potential of the support critically influence the spatial-temporal process, generating divergent morphologies and performances of PA layers [22-24].

Usually, the conventional polysulfone (PSf) or polyethersulfone (PES) ultrafiltration support membrane induces the rapid diffusion and uneven distribution of

amine monomers due to heterogeneous surface pore sizes and poor affinity. Diverse nano-materials have been applied as the interlayer to acquire ultra-thin selective layer, including carbon nanotubes (CNTs) [25-28], microporous organic nanotube (MONs) [20], graphitic carbon nitride (g-C_3N_4) [21], covalent organic frameworks (COFs) [29-31], metal organic frameworks (MOFs) [32, 33], MXenes [34], zeolites [35], cellulose nanocrystal (CNC) [36] and hydroxides [13, 37] etc. However, the aggregation and exfoliation of interlayer largely obstruct its scalable production and none of above candidates has been actually commercialized. Furthermore, PSf/PES ultrafiltration support membranes generally suffer from poor solvent stability, small pore size and high pore tortuosity, which increases the water transport pathway. Some studies utilize porous microfiltration membranes as the supports, such as polypropylene (PP) [38, 39], polyethylene (PE) [40], poly(vinylidene fluoride) (PVDF) [41], and polytetrafluoroethylene (PTFE) [42]. However, the hydrophobic essence of polymer materials is difficult to conduct IP reaction due to the uneven spread of the amine solution. These supports need further complicated hydrophilic modifications to enhance the interactions between the amine monomer and the substrate surface.

Meanwhile, the diffusion and reactivity of two-phase monomers will directly determine the crosslinking chemistry of PA layer. The utilization of typical piperazine (PIP) and 1,3,5-benzenetricarbonyl trichloride (TMC) leaves little manipulation room for improving separation performance due to restricted free volume and surface charged property [4, 43-50]. Guanidinium with primary amine groups was used to modify PA membranes for enhanced antifouling and antibacterial properties [51, 52]. Besides, the triaminoguanidine (TAG) molecule was applied as the single aqueous monomer to react with TMC to prepare positively charged PA membrane, which exhibited promising Li^+/Mg^{2+} sieving capability [53]. Molecular dynamics simulation validated that the

TAG molecule displayed a higher reactivity and a lower diffusivity than PIP [54].

Herein, we propose a facile and compelling strategy to prepare guanidyl-integrated PA NF membrane on the nylon porous support. The nylon microfiltration membrane is a highly suitable candidate as the support for IP owing to its large aperture, excellent wettability and solvent resistance. The favorable electrostatic interaction between the nylon substrate and amine monomers along with sufficient and even aqueous solution spread better manipulate IP process quest for high performance NF membranes. The second amine monomer, 1,3-diaminoguanidine (DAG) or TAG with divergent molecular structures and amino numbers, creates appropriate free volumes (equivalent radii of 4.60 Å and 3.85 Å) for fast water permeance without sacrificing molecules and ions selectivity, which breaks through the "trade-off" effect to some extent.

2. Methods

2.1. Materials and chemicals

Nylon porous supports (0.22 μm) were purchased from Shanghai Peninsula Industrial Co., Ltd. Purification Equipment Factory. The commercial polyether sulfone (PES), cellulose acetate (CA), hydrophilic modified polyvinylidene fluoride (PVDF) membranes with the average pore size of 0.22 μm were bought from Haiyan New Oriental Plastic Technology Co., Ltd. Piperazine (PIP, 99%), 1,3,5-Benzenetricarbonyl trichloride (TMC, 98%), triaminoguanidine hydrochloride (TAG·HCl, 97%), 1,3-diaminoguanidine hydrochloride (DAG·HCl, 97%), and polyethylene glycol (PEG) with a series of molecular weights were all purchased from Shanghai Aladdin Biochemical Technology Co., Ltd. n-hexane (97%) was from Shanghai Macklin Biochemical Co., Ltd. Inorganic salts including Na_2SO_4, $MgSO_4$, $CaCl_2$, $MgCl_2$, and NaCl (chemical pure) were from Sinopharm Chemical Reagent Co., Ltd (China). n-Hexane (97%) was from Shanghai Macklin Biochemical Co., Ltd. All the chemicals

were used without further purification.

2.2. Characterizations

The surface morphologies and the cross-section thickness of a series of membranes were investigated by scanning electron microscopy (FESEM, S4800, Hitachi) and transmission electron microscopy (TEM, JEOL2100, Japan). The membrane samples were embedded in cured epoxy and the ion beam apparatus (MODEL1, Gatan 695) was utilized to sectioning. Scanning probe microscope (Dimension ICON SPM, Bruker) in tapping mode were utilized to analyze the roughness of different as-prepared membranes as well as the atomic-scale interactions between PIP monomers and substrate surfaces. The detector tip was immersed in the PIP solution, meanwhile the tip adsorbed a certain amount of PIP molecules. When the tip approached and retracted away the surfaces of diverse substrates, the PIP-substrate interaction was built up.

The chemical components analysis and atomic concentrations of as-prepared membranes were characterized by X-ray photoelectron spectroscopy (XPS, Axis Ultra DLD, Kratos). Fourier transform infrared spectrometer (FTIR, NICOLET 6700) was applied to further characterize the chemical components of membranes. The hydrophilicity and wettability were measured using contact angle goniometer (OCA 25, Dataphysics). Zeta potentials for solid surface were evaluated by the electrolyte analyzer (SurPASS Anton Paar, GmbH) with 1 mM KCl solutions as electrolyte solution over a pH value range of 3-10. Total organic carbon analyzer (TOC, multi N/C2100) was used to reveal PEG concentrations in feed solution and filtrate. UV-vis spectroscopy was utilized to evaluate the maximum absorption peaks and absorbance of tetracycline. Besides, the concentrations of single-salt feed solution and filtrate were determined by electrical conductivity, obtained from electrical conductivity meter (DDSJ-308F, Shanghai leici instruments). Single-ion (such as Cl^- or SO_4^{2-})

concentration in the mixture was calculated from ion chromatography (IC, ICS1100, Thremo).

2.3. Preparation of guanidyl-integrated PA NF membranes

We chose the nylon, PES, CA or hydrophilic modified PVDF with the average aperture of 0.22 μm as the support membrane for IP. Taking DAG-incorporated PA membrane as an example, the nylon membrane with a diameter of 5 cm was placed on the sand core of the suction filter. 10 mL mixed aqueous solution containing PIP (0.2 w/v%) and DAG (12% of PIP content) was evenly poured onto the surface of nylon membrane. After two minutes, the redundant aqueous solution was removed and blotted with filter papers. 5 mL n-hexane solution of TMC with 0.1 w/v% was added onto the nylon support to initiate the IP reaction. After reacting 1 min, the oil phase solution was immediately poured away. The prepared PA NF membrane was thoroughly washed with n-hexane and was finally dried in an oven at 60 °C for 10 min. PA/nylon-M_1 represents the contrast PA NF membrane solely involving with PIP. PA/nylon-M_2 represents the PA NF membrane using DAG and PIP. PA/nylon-M_3 represents the PA NF membrane using TAG and PIP. The NF membrane was scaled up to 20*20 cm according to the same preparation methods (Fig. S1).

2.4. Desalination performance characterizations

Desalination performance of various PA NF membranes was evaluated by a cross-flow apparatus driven by pressure at room temperature. Effective filtration area of the cell was 3.14 cm^2. All as-prepared membranes were pre-compacted at 6.0 bar at least one hour using deionized water to reach stable permeance, then were tested at 5.0 bar. Feed solution permeance (P, LMH·bar^{-1}) was calculated by the following equation:

$$P=V/(Atp) \quad (1)$$

Where V (L) is the volume of collected filtrate, A (m^2) is the effective filtration

area, t is the measurement time interval (h) and p is the test pressure (bar).

The single-salt rejection (R) of as-prepared NF membranes with a series of saline solutions (Na_2SO_4, $MgSO_4$, $CaCl_2$, $MgCl_2$, and NaCl) were calculated by the formula as follows:

$$R = (C_f - C_p)/C_f \times 100\% \quad (2)$$

Where C_f is the solute concentration of feed solution and C_p is the solute concentration of filtrate. The solute concentrations were detected using the electrical conductivity meter due to the linear correlation between solute concentration and the conductivity.

The molecular weight cut off (MWCO) is identified by the rejection of 90% for spherical neutral solutes. Retention of the neutral solute represented by PEG with the molecular weights of 200, 300, 400, 600, 800, and 1000 Da was characterized by TOC. This calculation is consistent with formula (2), which C_f is the TOC concentration of feed solution and C_p is the TOC concentration of filtrate. The equivalent radius of free volume was calculated based on formula (3).

$$r_s = 16.73 \times 10^{-12} \times M_w^{0.557} \quad (3)$$

Where r_s (m) is the Stokes radius of PEG molecule and M_w is the MWCO of PEG molecule.

The single salt separation factor (S_{NaCl/Na_2SO_4}) and mixed ion separation factor ($S_{Cl^-/SO_4^{2-}}$) were applied to evaluate the monovalent/divalent ion selectivity, which can be calculated from equation (4) and (5):

$$S_{NaCl/Na_2SO_4} = (1-R_{NaCl})/(1-R_{Na_2SO_4}) \quad (4)$$

$$S_{Cl^-/SO_4^{2-}} = (1-R_{Cl^-})/(1-R_{SO_4^{2-}}) \quad (5)$$

Where R_{NaCl} and $R_{Na_2SO_4}$ separately represent the rejections of single NaCl and

Na_2SO_4. R_{Cl^-} and $R_{SO_4^{2-}}$ represent the rejections of Cl^- and SO_4^{2-} in NaCl/Na_2SO_4 binary saline solution. The single salt concentration of NaCl or Na_2SO_4 was 1000 ppm. The total concentration of mixed saline solution was 2000 ppm and the mass ratio of NaCl to Na_2SO_4 was 1:1.

3. Results and discussion

3.1. Guanidyl-integrated PA NF membranes

3.1.1. Surface morphology of PA/nylon-M_x

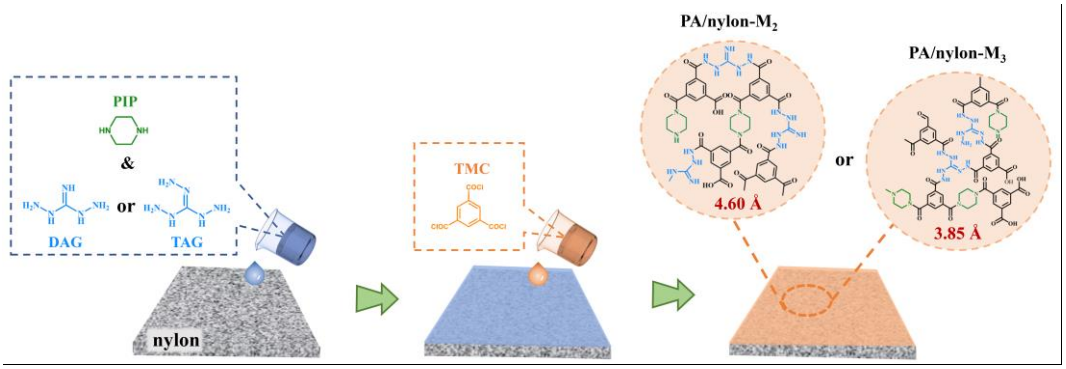

Scheme 1. Preparation process of PA/nylon-M_x NF membrane. DAG and TAG involved NF membranes were termed as PA/nylon-M_2 and PA/nylon-M_3, respectively. PA/nylon-M_1 was used as a control sample without guanidinium.

In contrast to the binary PIP and TMC in the IP reaction, guanidyl-integrated PA NF membranes were created by introducing the second amine monomer (DAG or TAG) as shown in Scheme 1. DAG and TAG molecules own diverse molecular structures and active amino groups. The PA network structure could be manipulated by DAG or TAG at sub-angstrom scale. All PA/nylon membranes displayed similar surface morphologies featuring smooth and nodular structure like "calm sea and raised island" (Fig. 1a-1c). The morphologies were mainly caused by the heat releasing effect in the process of IP, especially at the relatively large pore support. The beneath macropores create free liquid-liquid interface that allows degassed nanobubbles created during IP process to easily escape, thus generating the "calm sea". Meanwhile, the "raised island"

part was created by the confinement interface between the substrate and PA film in view that the resulting microbubbles cannot well escape from the solid-liquid interface [23, 55]. The free interfacial part of large pore fairly shortened the transverse transfer distance and declined the transfer resistance between the PA layer and the nylon support, thus facilitating the fast water transport.

The thickness of PA films of PA/nylon-M_2 and PA/nylon-M_3 were both less than 50 nm that were thinner than PA/nylon-M_1 (Fig. 1d-1i). The diffusion rate of DAG or TAG was slowed down to acquire relatively thinner PA layer possibly due to the stronger interaction of multiple amino groups with the negatively charged nylon substrate. (The selection and spatial-temporal regulation of the nylon substrate will be discussed in Section 3.2 in detail). The AFM results showed the roughness of PA/nylon-M_2 and PA/nylon-M_3 were lower than PA/nylon-M_1, implying that guanidinium involved IP process were more controllable (Fig. S2).

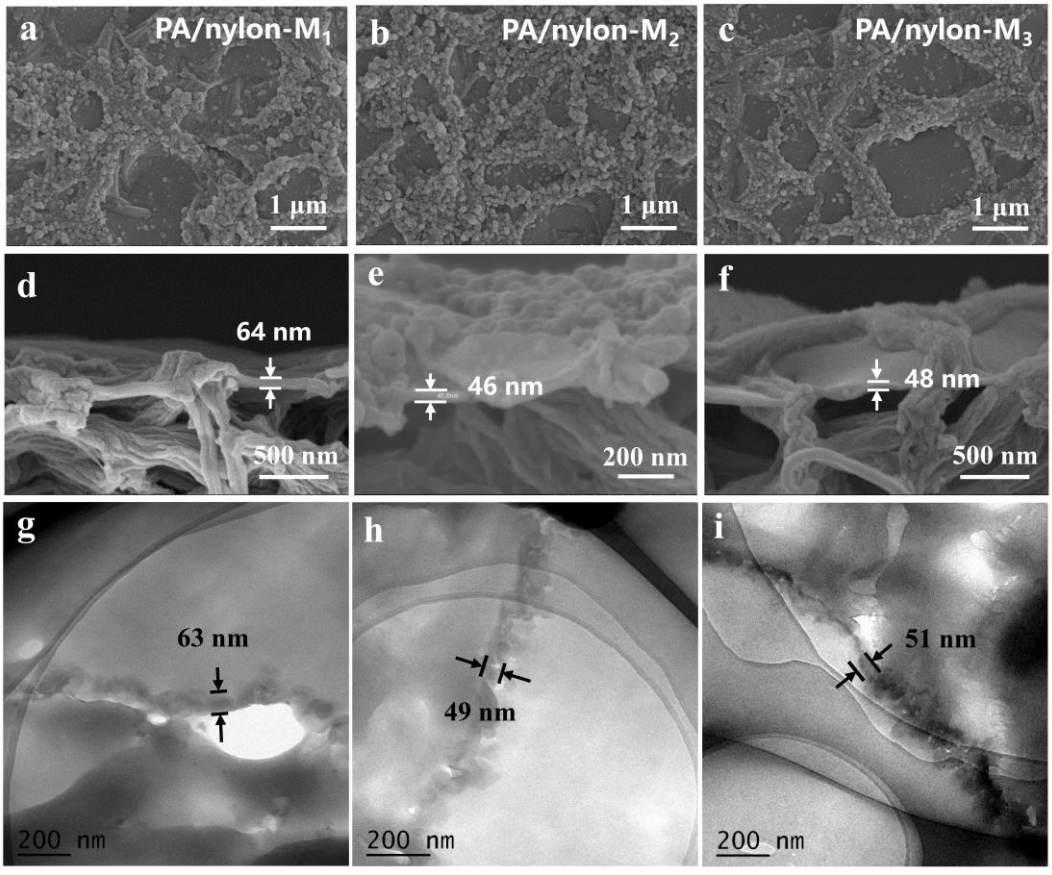

Fig. 1. Surface morphologies and thickness of PA/nylon-M_x. (a-c) SEM images of PA/nylon-M_1, PA/nylon-M_2, and PA/nylon-M_3. (d-f) Cross-section SEM images of PA/nylon-M_1, PA/nylon-M_2, and PA/nylon-M_3. (g-i) TEM images of PA/nylon-M_1, PA/nylon-M_2, and PA/nylon-M_3.

3.1.2 Physicochemical properties of PA/nylon-M_x

The chemical compositions of diverse PA NF membranes were intensively characterized by XPS and FTIR. From Fig. 2, the high-resolution C 1s deconvolution spectra showed that three peaks respectively associated with C-C/C-H at 284.6 eV, C-N at 285.7 eV, and C=O at 287.6 eV further confirmed the formation of PA film. The N 1s spectra exhibited that the PA active layers of PA/nylon-M_2 and PA/nylon-M_3 still retained more amino groups present in DAG and TAG molecules. The N-H peak contents of PA/nylon-M_2 and PA/nylon-M_3 were respectively 13.9% and 25.0% (Fig. 2e, and 2f). The density of amine group present in PA/nylon-M_3 was higher than PA/nylon-M_2, indicating TAG had a greater reaction and crosslinking extent. The same peak content present in PA/nylon-M_1 was only 5.6% (Fig. 2d). Moreover, the atomic/mass concentrations of element N of PA/nylon-M_2 and PA/nylon-M_3 were higher than PA/nylon-M_1, suggesting that the guanidinium were involved in the IP reaction (see Table S1). The O 1s deconvolution spectra showed the similar peak-splitting situations of the three membranes. The carboxyl content arising from the hydrolysis of underreacted acyl chloride in PA/nylon-M_2 was the highest, which indicated the lower reaction degree of TMC. (Fig. 2g-2i). The functional group of the nylon substrate is amido bond, -CONH-, which is consistent with the major composition of PA layer. The peak located at 3296 cm^{-1} was attributed to the stretching vibration of N-H. The obvious peaks located at 1634 cm^{-1} and 1540 cm^{-1} were the amide □ band (the stretching vibration of C=O) and amide □ band (the bending vibration of

N-H). The distinction was the range of 3200 cm^{-1}~3600 cm^{-1} which was due to the occurrence of amino and carboxyl, especially present in PA membranes. The new peak at 1440 cm^{-1} was originated from the aromatic ring present in aromatic polyamide (Fig. S3). In addition, the elements C/N/O were uniformly distributed on the surfaces of PA/nylon-M_x (Fig. S4).

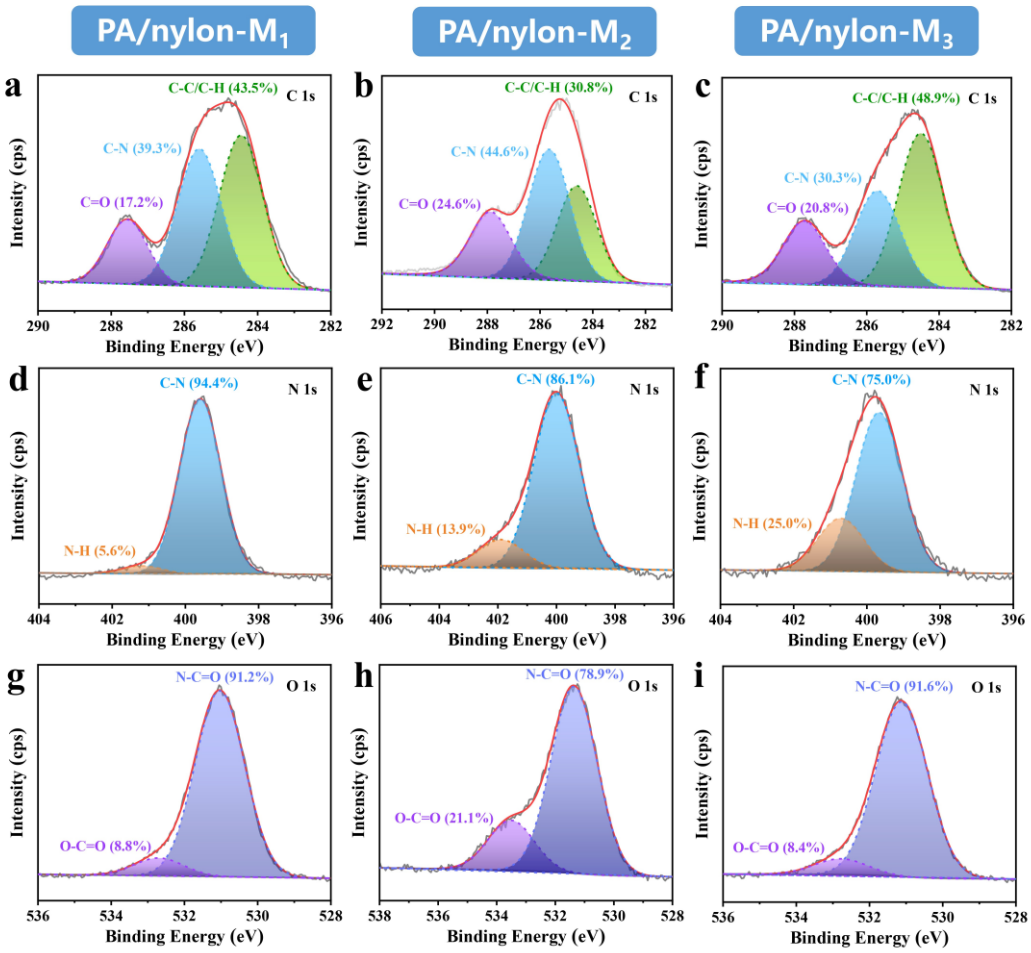

Fig. 2. XPS analysis of PA/nylon-M_x. (a-c) High-resolution XPS spectra of C 1s with PA/nylon-M_1, PA/nylon-M_2, and PA/nylon-M_3. (d-f) High-resolution XPS spectra of N 1s with PA/nylon-M_1, PA/nylon-M_2, and PA/nylon-M_3. (g-i) High-resolution XPS spectra of O 1s with PA/nylon-M_1, PA/nylon-M_2, and PA/nylon-M_3.

Size exclusion and Donnan effect are usually accepted mechanisms in the field of nanofiltration desalination. The hydrophilicity, surface charged property and transfer

pore size of selective layer play pivotal roles in NF process. As shown in WCA characterization, the water wettability of PA/nylon-M_2 and PA/nylon-M_3 was improved. PA/nylon-M_2 expressed better hydrophilicity than other two membranes (Fig. 3a), favoring the fast water diffusion and transport through the membrane. From Fig. 3b, we can see that PA/nylon-M_2 and PA/nylon-M_3 showed relatively higher zeta potentials than PA/nylon-M_1 at pH<7. It was because the more amine groups present in PA/nylon-M_2 and PA/nylon-M_3 occurred protonation in the acidic solution. At pH>7, PA/nylon-M_2 showed the strongly negatively charged surface property due to the deprotonation of carboxyl groups, consistent with the results of O 1s spectrum (Fig. 3b). The higher content of carboxyl group on the surface caused more negative surface. The underreacted acyl chloride groups were attributed to the molecular structure of DAG.

DAG monomer with two-arm primary amine groups shows larger molecular dimension than PIP as shown in the-ball-and-stick model and molecular formula of sectional structure unit (Fig. 3d). The distance between the carbons of two acyl chloride monomers is 6.9 Å or 6.1 Å due to the various configuration of DAG monomer, which is longer than PIP with 5.6 Å. Likewise, TAG as a three-arms molecule holds 3 reaction sites with shorter distance (3.5 Å) and larger crosslinking degree (Fig. 3e). Therefore, the free volume of polyamide can be changed at sub-angstrom scale by introducing DAG/TAG molecules. Besides, “two-arms” DAG molecule has lower contact and reaction probability than “three arms” TAG molecule, resulting in insufficient utilization of acyl chloride groups of TMC and loose crosslinking structure of PA/nylon-M_2. The MWCO (383 Da) of PA/nylon-M_2 was higher than that of PA/nylon-M_1 (256 Da) and PA/nylon-M_3 (279 Da) as illustrated in Fig. 3c. We further calculated the equivalent aperture radii of PA/nylon-M_x according to the formula (3). The equivalent radii of free volume of PA/nylon-M_1, PA/nylon-M_2 and PA/nylon-M_3 are

respectively 3.67 Å, 4.60 Å and 3.85 Å. Thus, the free volume of PA NF membranes could be precisely manipulated at sub-angstrom scale by guanidinium involved interfacial polymerization.

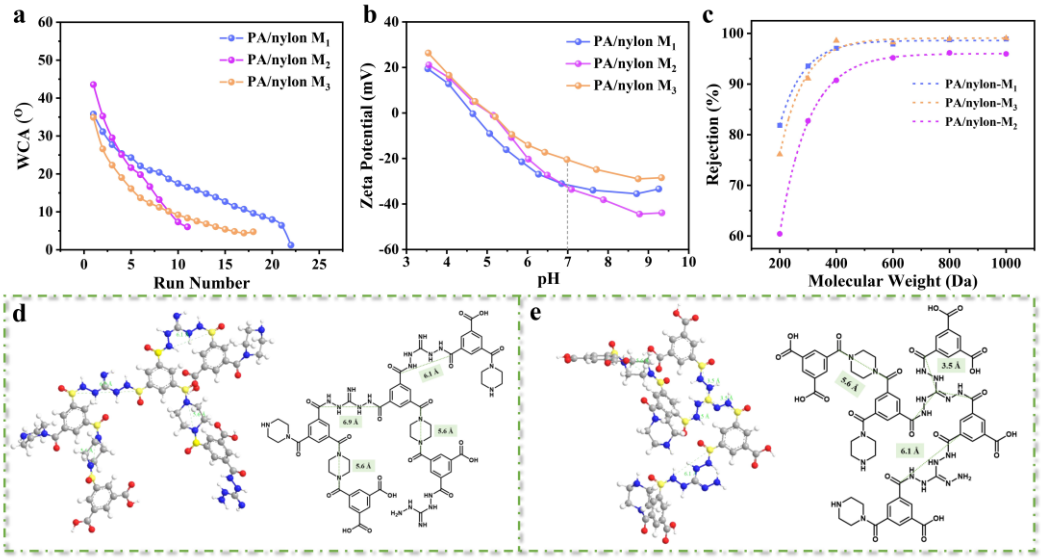

Fig. 3. (a) Water contact angles of PA/nylon-M_x. (b) Zeta potentials for solid surfaces of PA/nylon-M_x. (c) Molecular weight cut off (MWCO) of PA/nylon-M_x. (d) Molecular formula and the-ball-and-stick model of crosslinking structural fragment of PA/nylon-M_2. (e) Molecular formula and the-ball-and-stick model of crosslinking structural fragment of PA/nylon-M_3.

3.2 Role of nylon microfiltration support membrane

The pore sizes, porosity, wettability, and exterior physicochemical properties of support membranes provide a pivotal link to the formation of PA active layer by IP along with desalination performance of PA NF membrane. We further selected four substrates containing nylon, PES, CA and hydrophilic modified PVDF membranes with average aperture of 0.22 μm to investigate the roles of the microporous substrate on NF performance (Fig. S5). The formed PA layers displayed similar surface morphologies combining smooth and nodular constructions, which was ascribed to the free interface and confinement interface effects (Fig.4). Meanwhile, DAG/TAG-incorporated

composite PA NF membranes were characterized by SEM and AFM. The morphologies of guanidyl-integrated PA layers with different polymer substrates are similar to conventional PA layers formed by TMC and PIP (Fig. S6 and S7).

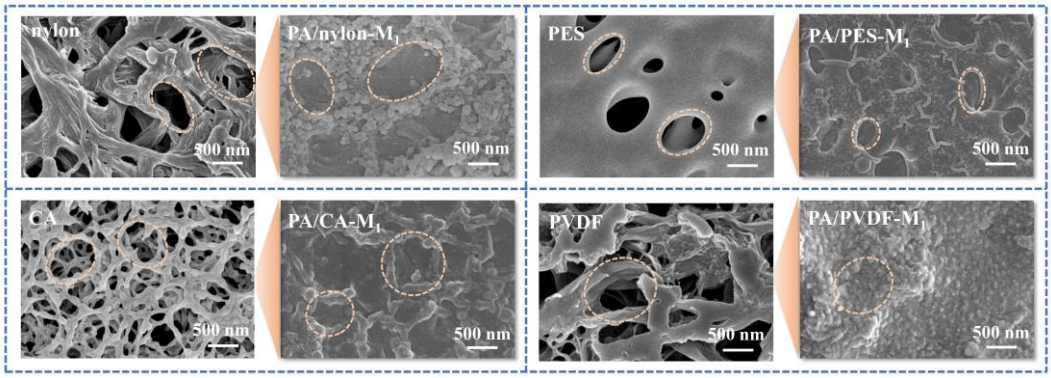

Fig. 4. SEM images of four substrates, respectively containing nylon, PES, CA, and PVDF membranes as well as SEM images of the conventional PA membranes with above four substrates that were named as PA/nylon-M_1, PA/PES-M_1, PA/CA-M_1, and PA/ PVDF-M_1 membranes.

Spatial-temporal distribution and diffusion of aqueous monomers are of vital significance to realize highly perm-selective NF membranes. Positively charged PIP molecules can adequately adsorbed and evenly distributed on the electronegative support surface through long-range electrostatic interaction for controllable diffusion and reaction (Fig. 5a). The hydrophilic and highly porous substrate is favorable to absorb and store sufficient PIP solution for subsequent reaction (Fig. 5b). We further investigated the atomic-scale interaction force between PIP molecules and substrate surface by AFM. As shown in Fig. 5c, the force-distance curves quantitatively showed the magnitude of interactions between PIP molecules and different substrates. The nylon membrane showed the highest drag force (F_{max}=0.70 nN) and interaction range compared to other membranes.

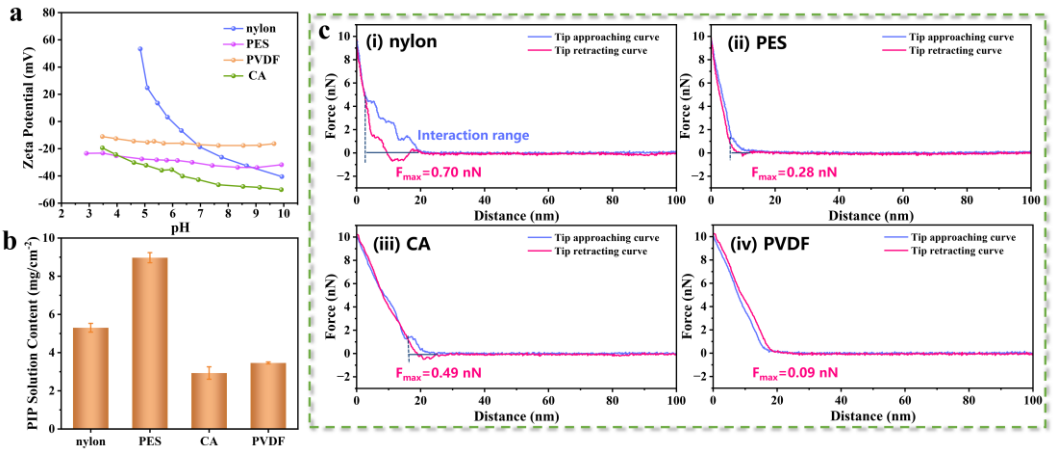

Fig. 5. (a) Zeta potentials for solid surface of four support membranes. (b) Adsorption content of the PIP solution of different support membranes. (c) Force-distance curves of PIP monomers with diverse wetting substrate surfaces of nylon (i), PES (ii), CA (iii), and PVDF (iv). The atomic-scale interaction force was evaluated.

Hence, PA/nylon-M_1 showed outstanding permselectivity compared with other PA composite membranes with divergent supports. The rejection of Na_2SO_4 could reach over 99% (Fig. S8). Also, the water permeance of PA/nylon-M_2 greatly increased to twice of PA/nylon-M_1, which is higher than other composite membranes as depicted in Fig. S8b.

3.3 Desalination performance of PA/nylon-M_x

In order to validate the permselectivity of guanidyl-integrated NF membranes, we performed a series of single salt and mixed ions separation measurements. All as-prepared membranes were operated under the cross-flow condition driven by pressure of 5 bar. Firstly, the preparation condition of PA/nylon-M_2 were optimized by varying contents of DAG monomers. In case of DAG (12% of PIP content) involved in IP, the water permeance of PA/nylon-M_2 could reach 46.5 LHM·bar^{-1} and the rejection of Na_2SO_4 was up to 95% (Fig. S9). Likewise, the water permeance of PA/nylon-M_3 was enhanced to 33.1 LHM·bar^{-1}. Therefore, the permeance of two guanidyl-integrated NF membranes were strongly improved. Moreover, given that PA/nylon-M_3 reserved

smaller pore size than PA/nylon-M_2, the rejection of Na_2SO_4 was increased to 99.2%, which had almost no attenuation than PA/nylon-M_1 (Fig. 6a).

We further examined the rejection of diverse salts, including Na_2SO_4, $MgSO_4$, $CaCl_2$, $MgCl_2$, and NaCl to evaluate the desalination capabilities of three PA NF membranes (Fig. 6b). PA/nylon-M_1 and PA/nylon-M_3 showed outstanding interception abilities of divalent anionic salts according to size exclusion and Donnan effect. Theoretically, the hydrated radii of SO_4^{2-} and Cl^- are respectively 3.79 Å and 3.32 Å. The size of SO_4^{2-} and Cl^- is only sub-angstrom difference, but SO_4^{2-} owns more negative charges than Cl^- in the feed solution. Therefore, PA/nylon-M_1 (3.67 Å) can effectively sieve SO_4^{2-} and Cl^-. Although the equivalent radius of free volume of PA/nylon-M_3 (3.85 Å) is a little larger than the hydrated radius of SO_4^{2-}, the negatively charged surface is beneficial to reject high-valence co-ions, meanwhile screening corresponding counterions. Therefore, the synergistic effects of steric and charged exclusion guarantee the rejection of high-valent anionic salts, such as Na_2SO_4 and $MgSO_4$. The Na_2SO_4 rejections of PA/nylon-M_1 and PA/nylon-M_3 were 99.4% and 99.2%. The $MgSO_4$ rejections of PA/nylon-M_1 and PA/nylon-M_3 were 98.4% and 97.8%. In addition, the rejection of $CaCl_2$, $MgCl_2$, or NaCl of PA/nylon-M_3 was a little higher than PA/nylon-M_1 on account that the slightly acidic condition in saline solution protonated part of amino groups, which led to the rejection of cations. Although the Na_2SO_4 rejection of PA/nylon-M_2 was relatively weak, the saline permeance of PA/nylon-M_2 was greatly improved than the contrast sample, PA/nylon-M_1. Therefore, PA/nylon-M_2 is conductive to efficiently removing larger molecules and high-valence heavy metal ions in pursuit of high flux (Table S2). Further, we conducted the single salt selectivity as well as mixed anions selectivity of PA/nylon-M_x. As demonstrated in Fig. 6c, the PA/nylon-M_3 shows the comprehensive outstanding permselectivity in terms of NaCl/

Na_2SO_4 selectivity, Cl^-/SO_4^{2-} selectivity and permeance, surpassing the state-of-the-art PA NF membranes (Fig. 6d).

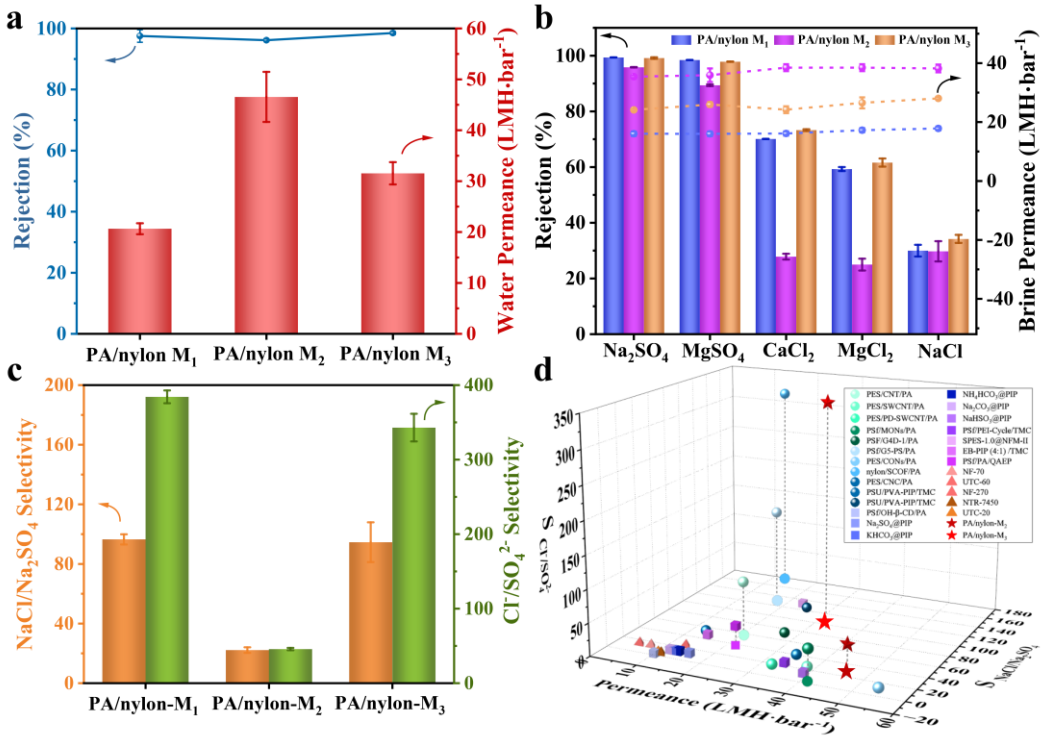

Fig. 6. (a) Na_2SO_4 rejection and water permeance of PA/nylon-M_x. (b) Different saline rejection and permeance of PA/nylon-M_x; (c) Single salt (NaCl/ Na_2SO_4) selectivity and mixed salts (Cl^-/SO_4^{2-}) selectivity of PA/nylon-M_x. (d) Comparison of separation performances of reported typical NF membranes and this work. Circular legends represent NF membranes with interlayers; rectangle legends represent that PA layers created by IP reaction system with multiple monomers or components; triangle legends represent commercial NF membranes (detail statistics are shown in Table S3).

The DAG-regulated IP reaction creates the thin and loose PA layer, which contributes to certain selectivity and high permeance of PA/nylon-M_2. With the increasing concentration of Na_2SO_4 solution from 1000 ppm to 5000 ppm, the salt rejection of PA/nylon-M_2 remained stable. The decline of permeance was attributed to concentration polarization, but the permeance maintained more than 20 LHM·bar^{-1} (Fig. 7a). From the above discussion, the PA/nylon-M_3 showed splendid permselectivity and

mono/divalent anions sieving capability. Apart from that, the PA/nylon-M_3 can achieve effective tetracycline interception. The rejection ratios of a series of tetracycline solutions from 3 ppm to 12 ppm were 100%, which provides a satisfactory removal and recovery of antibiotics (Fig. 7c).

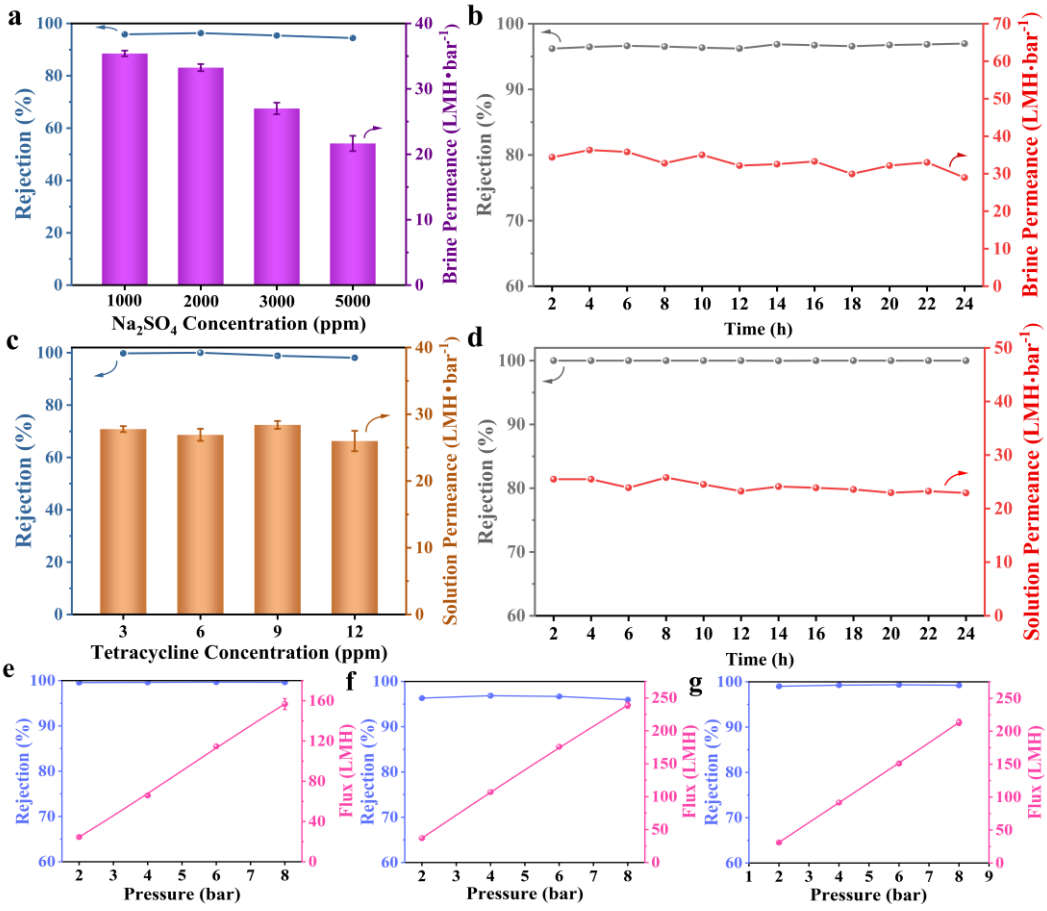

Fig. 7. (a) Na_2SO_4 rejection and permeance of PA/nylon-M_2 with the increasing salt concentrations. (b) Long-term operational stability of PA/nylon-M_2 with 1000 ppm Na_2SO_4 solution as the feed solution. (c) Tetracycline rejection and permeance of PA/nylon-M_3 with the different tetracycline concentrations. (d) Long-term operational stability of PA/nylon-M_3 with 3 ppm tetracycline solution as the feed solution. (e-g) The anti-pressure performances under cross-flow condition with the linearly increased pressure of PA/nylon-M_1 (e), PA/nylon-M_2 (f), and PA/nylon-M_3 (g).

To further explore the operational stability, we tested the guanidyl-integrated PA NF

membranes for consecutive 24 h. As shown in Fig. 7b and 7d, PA/nylon-M_2 showed a quite stable rejection of Na_2SO_4 around 96% and high permeance. Similarly, the PA/nylon-M_3 maintained high removal efficiency (100%) of tetracycline over 24 h. The excellent interface compatibility between the PA selective layer and nylon substrate offers long-term operational stability.

In addition, we studied the pressure resistance of NF membranes with nylon support. The flux of PA/nylon-M_x enhanced linearly with increasing the operational pressure up to 8 bar, meanwhile the rejection of Na_2SO_4 was almost constant (Fig. 7e-g). More attractively, the nylon based composite PA membrane showed good resistance to different polar and non-polar organic solvents. The result displayed that the permeance of polar solvents by PA/nylon-M_2 was related to the molecular sizes and the non-polar solvents remained impenetrable under pressure. The permeances of polar solvents containing methanol, ethanol, and acetonitrile are respectively 21.4, 6.3, and 11.1 LHM·bar^{-1} (Fig. S10), which displaying the desirable potential of separating polar/non-polar organic solvents.

4. Conclusion

In summary, we provided a facile and scalable strategy to construct high-permselectivity PA NF membranes by directly introducing guanidinium (DAG or TAG) into amine aqueous solution for interfacial polymerization. The nylon microfiltration membrane was used as the support due to the desirable negatively charged surface, high monomer storage and the favorable interactions. DAG and TAG with divergent molecular sizes and amino structures created various free volumes (pore sizes) of PA/nylon-M_2 and PA/nylon-M_3. By contrast to the PA/nylon-M_1, the water permeance of PA/nylon-M_2 got extreme increment to 46.5 LHM·bar^{-1} and the rejection of Na_2SO_4 was higher than 95%. The permeance of PA/nylon-M_3 increased up to 30 LHM·bar^{-1},

meanwhile maintaining prominent rejection of Na_2SO_4 (99.2%), surpassing most of the "state-of-the-art" PA NF membranes. In addition, PA/nylon-M_3 showed splendid mono/divalent anion sieving and 100% tetracycline removal capabilities. The guanidyl-integrated nylon composite NF membranes open a new avenue for effective desalination, water advanced treatment and organic solvent nanofiltration.

Author contribution statement

Shuting Xu: Conceptualization, Data curation, Experimental investigation, Methodology, Writing – original draft.

Jiahuan Liu: Data curation, Experimental investigation.

Jianqiang Wang: Methodology, Project administration.

Haibo Lin: Experimental guidance, Formal analysis.

Qiu Han: Experimental guidance, Formal analysis.

Fu Liu: Supervision, Methodology, Writing-review & editing, Funding acquisition, Project administration, Resources.

Chuyang Y. Tang: Methodology, Writing-review & editing.

Declaration of competing interest

The authors declare that they have no known competing financial interests or personal relationships that could have appeared to influence the work reported in this paper.

Data availability

Data will be made available on request

Acknowledgments

This work is financially supported by Ningbo International R&D Collaboration Project (2023H001), International Partnership Program of Chinese Academy of Sciences-Grand Challenges (No. 181GJHZ2022038GC), National Natural Science Foundation of China (No. 51973230), Distinguished Young Scholars of Zhejiang Province (LR20E030002), Ten Thousand Plan-high Level Talents Special Support Plan of Zhejiang province, China (ZJWR0108020).

References:

[1] C. He, Z. Liu, J. Wu, X. Pan, Z. Fang, J. Li, B. A. Bryan, Future global urban water scarcity and potential solutions, Nat. Commun. 12 (2021) 4667. http://doi.org/10.1038/s41467-021-25026-3

[2] M. Elimelech, W. A. Phillip, The future of seawater desalination energy technology and the environment, Science 333 (2011) 712-717. https://www.science.org/doi/10.1126/science.1200488.

[3] A. W. Mohammad, Y. H. Teow, W. L. Ang, Y. T. Chung, D. L. Oatley-Radcliffe, N. Hilal, Nanofiltration membranes review: Recent advances and future prospects, Desalination 356 (2015) 226-254. http://doi.org/10.1016/j.desal.2014.10.043

[4] W. Fang, L. Shi, R. Wang, Mixed polyamide-based composite nanofiltration hollow fiber membranes with improved low-pressure water softening capability, J. Membr. Sci. 468 (2014) 52-61. http://doi.org/10.1016/j.memsci.2014.05.047

[5] E. L. Wittbecker, P. W. Morgan, Interfacial polycondensation. I., J. Polym. Sci. 40 (1959) 289-297. http://doi.org/10.1002/pol.1959.1204013701

[6] L. Shen, R. Cheng, M. Yi, W. S. Hung, S. Japip, L. Tian, X. Zhang, S. Jiang, S. Li, Y. Wang, Polyamide-based membranes with structural homogeneity for ultrafast molecular sieving, Nat. Commun. 13 (2022) 500. http://doi.org/10.1038/s41467-022-

476 28183-1
477 [7] H. Guo, X. Li, W. Yang, Z. Yao, Y. Mei, L. E. Peng, Z. Yang, S. Shao, C. Y. Tang,
478 Nanofiltration for drinking water treatment: A review, Front. Chem. Sci. Eng. 16 (2022)
479 681-698. http://doi.org/10.1007/s11705-021-2103-5
480 [8] Z. Yang, H. Guo, C. Y. Tang, The upper bound of thin-film composite (TFC)
481 polyamide membranes for desalination, J. Membr. Sci. 590 (2019) 117297.
482 http://doi.org/10.1016/j.memsci.2019.117297
483 [9] G. M. Geise, H. B. Park, A. C. Sagle, B. D. Freeman, J. E. McGrath, Water
484 permeability and water/salt selectivity tradeoff in polymers for desalination, J. Membr.
485 Sci. 369 (2011) 130-138. http://doi.org/10.1016/j.memsci.2010.11.054
486 [10] G. M. Geise, D. R. Paul, B. D. Freeman, Fundamental water and salt transport
487 properties of polymeric materials, Prog. Polym. Sci. 39 (2014) 1-42.
488 http://doi.org/10.1016/j.progpolymsci.2013.07.001
489 [11] Z. Yang, L. Long, C. Wu, C. Y. Tang, High permeance or high selectivity?
490 Optimization of system-scale nanofiltration performance constrained by the upper
491 bound, ACS ES&T Eng. 2 (2021) 377-390. http://doi.org/10.1021/acsestengg.1c00237
492 [12] B. Yuan, S. Zhao, P. Hu, J. Cui, Q. J. Niu, Asymmetric polyamide nanofilms with
493 highly ordered nanovoids for water purification, Nat. Commun. 11 (2020) 6102.
494 http://doi.org/10.1038/s41467-020-19809-3
495 [13] S. Karan, Z. Jiang, A. G. Livingston, Sub–10 nm polyamide nanofilms with
496 ultrafast solvent transport for molecular separation, Science 348 (2015) 1347-1351.
497 [14] C. Jiang, L. Tian, Z. Zhai, Y. Shen, W. Dong, M. He, Y. Hou, Q. J. Niu, Thin-film
498 composite membranes with aqueous template-induced surface nanostructures for
499 enhanced nanofiltration, J. Membr. Sci. 589 (2019).
500 http://doi.org/10.1016/j.memsci.2019.117244

501 [15] Y. Liang, Y. Zhu, C. Liu, K. R. Lee, W. S. Hung, Z. Wang, Y. Li, M. Elimelech, J.
502 Jin, S. Lin, Polyamide nanofiltration membrane with highly uniform sub-nanometre
503 pores for sub-1 a precision separation, Nat. Commun. 11 (2020) 2015.
504 http://doi.org/10.1038/s41467-020-15771-2
505 [16] Z. Tan, S. Chen, X. Peng, L. Zhang, C. Gao, Polyamide membranes with nanoscale
506 turing structures for water purification, Science 360 (2018) 518-521.
507 https://www.science.org/doi/10.1126/science.aar6308
508 [17] H. Zhang, Q. He, J. Luo, Y. Wan, S. B. Darling, Sharpening nanofiltration:
509 Strategies for enhanced membrane selectivity, ACS Appl. Mater. Interfaces 12 (2020)
510 39948-39966. http://doi.org/10.1021/acsami.0c11136
511 [18] Z. Yang, Z. W. Zhou, H. Guo, Z. Yao, X. H. Ma, X. Song, S. P. Feng, C. Y. Tang,
512 Tannic acid/Fe(3+) nanoscaffold for interfacial polymerization: Toward enhanced
513 nanofiltration performance, Environ. Sci. Technol. 52 (2018) 9341-9349.
514 http://doi.org/10.1021/acs.est.8b02425
515 [19] X. You, K. Xiao, H. Wu, Y. Li, R. Li, J. Yuan, R. Zhang, Z. Zhang, X. Liang, J.
516 Shen, Z. Jiang, Electrostatic-modulated interfacial polymerization toward ultra-
517 permselective nanofiltration membranes, iScience 24 (2021) 102369.
518 http://doi.org/10.1016/j.isci.2021.102369
519 [20] S. Han, J. Zhu, A. A. Uliana, D. Li, Y. Zhang, L. Zhang, Y. Wang, T. He, M.
520 Elimelech, Microporous organic nanotube assisted design of high performance
521 nanofiltration membranes, Nat. Commun. 13 (2022) 7954.
522 http://doi.org/10.1038/s41467-022-35681-9
523 [21] C. Zhao, Y. Zhang, Y. Jia, B. Li, W. Tang, C. Shang, R. Mo, P. Li, S. Liu, S. Zhang,
524 Polyamide membranes with nanoscale ordered structures for fast permeation and highly
525 selective ion-ion separation, Nat. Commun. 14 (2023) 1112.

http://doi.org/10.1038/s41467-023-36848-8

[22] X. Li, Q. Li, W. Fang, R. Wang, W. B. Krantz, Effects of the support on the characteristics and permselectivity of thin film composite membranes, J. Membr. Sci. 580 (2019) 12-23. http://doi.org/10.1016/j.memsci.2019.03.003

[23] L. E. Peng, Z. Yao, Z. Yang, H. Guo, C. Y. Tang, Dissecting the role of substrate on the morphology and separation properties of thin film composite polyamide membranes: Seeing is believing, Environ. Sci. Technol. 54 (2020) 6978-6986. http://doi.org/10.1021/acs.est.0c01427

[24] R. Dai, Z. Yang, Z. Qiu, L. Long, C. Y. Tang, Z. Wang, Distinct impact of substrate hydrophilicity on performance and structure of TFC NF and RO polyamide membranes, J. Membr. Sci. 662 (2022) 120966. http://doi.org/10.1016/j.memsci.2022.120966

[25] Y. Zhu, W. Xie, S. Gao, F. Zhang, W. Zhang, Z. Liu, J. Jin, Single-walled carbon nanotube film supported nanofiltration membrane with a nearly 10 nm thick polyamide selective layer for high-flux and high-rejection desalination, Small 12 (2016) 5034-5041. http://doi.org/10.1002/smll.201601253

[26] Z. Zhou, Y. Hu, C. Boo, Z. Liu, J. Li, L. Deng, X. An, High-performance thin-film composite membrane with an ultrathin spray-coated carbon nanotube interlayer, Environ. Sci. Technol. Lett. 5 (2018) 243-248. http://doi.org/10.1021/acs.estlett.8b00169

[27] S. Gao, Y. Zhu, Y. Gong, Z. Wang, W. Fang, J. Jin, Ultrathin polyamide nanofiltration membrane fabricated on brush-painted single-walled carbon nanotube network support for ion sieving, ACS Nano 13 (2019) 5278-5290. http://doi.org/10.1021/acsnano.8b09761

[28] G. Gong, P. Wang, Z. Zhou, Y. Hu, New insights into the role of an interlayer for the fabrication of highly selective and permeable thin-film composite nanofiltration

membrane, ACS Appl. Mater. Interfaces 11 (2019) 7349-7356. http://doi.org/10.1021/acsami.8b18719

[29] J. Yuan, M. Wu, H. Wu, Y. Liu, X. You, R. Zhang, Y. Su, H. Yang, J. Shen, Z. Jiang, Covalent organic framework-modulated interfacial polymerization for ultrathin desalination membranes, J. Mater. Chem. A 7 (2019) 25641-25649. http://doi.org/10.1039/c9ta08163a

[30] Z. Zhang, X. Shi, R. Wang, A. Xiao, Y. Wang, Ultra-permeable polyamide membranes harvested by covalent organic framework nanofiber scaffolds: A two-in-one strategy, Chem. Sci. 10 (2019) 9077-9083. http://doi.org/10.1039/c9sc03088c

[31] S. Xu, H. Lin, G. Li, J. Wang, Q. Han, F. Liu, Anionic covalent organic framework as an interlayer to fabricate negatively charged polyamide composite nanofiltration membrane featuring ions sieving, Chem. Eng. J. 427 (2022). http://doi.org/10.1016/j.cej.2021.132009

[32] Z. Wang, Z. Wang, S. Lin, H. Jin, S. Gao, Y. Zhu, J. Jin, Nanoparticle-templated nanofiltration membranes for ultrahigh performance desalination, Nat. Commun. 9 (2018) 2004. http://doi.org/10.1038/s41467-018-04467-3

[33] S. Han, Z. Wang, S. Cong, J. Zhu, X. Zhang, Y. Zhang, Root-like polyamide membranes with fast water transport for high-performance nanofiltration, J. Mater. Chem. A 8 (2020) 25028-25034. http://doi.org/10.1039/d0ta06520j

[34] Q. Li, T. Zhang, Z. Dai, F. Su, X. Xia, P. Dong, J. Zhang, A novel positively charged nanofiltration membrane stimulated by amino-functionalized MXene $Ti_3C_2T_x$ for high rejection of water hardness ions, J. Membr. Sci. 671 (2023) 121385. http://doi.org/10.1016/j.memsci.2023.121385

[35] D. Wang, M. Tian, S. Han, K. Ding, L. Yin, J. Zhu, Y. Zhang, L. Han, Enhanced performance of thin-film nanocomposite membranes achieved by hierarchical zeolites

for nanofiltration, J. Membr. Sci. 671 (2023) 121405. http://doi.org/10.1016/j.memsci.2023.121405

[36] J.-J. Wang, H.-C. Yang, M.-B. Wu, X. Zhang, Z.-K. Xu, Nanofiltration membranes with cellulose nanocrystals as an interlayer for unprecedented performance, J. Mater. Chem. A 5 (2017) 16289-16295. http://doi.org/10.1039/c7ta00501f

[37] P. Li, B. Wei, Z. Yao, P. Li, Y. Hou, Y. Yang, Q. J. Niu, Nanorod-interlayered thin film composite membranes for ultrafast nanofiltration, Desalination 548 (2023) 116255. http://doi.org/10.1016/j.desal.2022.116255

[38] H. I. Kim, S. S. Kim, Plasma treatment of polypropylene and polysulfone supports for thin film composite reverse osmosis membrane, J. Membr. Sci. 286 (2006) 193-201. http://doi.org/10.1016/j.memsci.2006.09.037

[39] A. P. Korikov, P. B. Kosaraju, K. K. Sirkar, Interfacially polymerized hydrophilic microporous thin film composite membranes on porous polypropylene hollow fibers and flat films, J. Membr. Sci. 279 (2006) 588-600. http://doi.org/10.1016/j.memsci.2005.12.051

[40] S. H. Park, Y. J. Kim, S. J. Kwon, M. G. Shin, S. E. Nam, Y. H. Cho, Y. I. Park, J. F. Kim, J. H. Lee, Polyethylene battery separator as a porous support for thin film composite organic solvent nanofiltration membranes, ACS Appl. Mater. Interfaces. 10 (2018) 44050-44058. http://doi.org/10.1021/acsami.8b16403

[41] E.-S. Kim, Y. J. Kim, Q. Yu, B. Deng, Preparation and characterization of polyamide thin-film composite (TFC) membranes on plasma-modified polyvinylidene fluoride (PVDF), J. Membr. Sci. 344 (2009) 71-81. http://doi.org/10.1016/j.memsci.2009.07.036

[42] X. Zhang, T. Li, Z. Wang, J. Wang, S. Zhao, Polar aprotic solvent-resistant nanofiltration membranes generated by flexible-chain binding interfacial

601 polymerization onto PTFE substrate, J. Membr. Sci. 668 (2023) 121294.
602 http://doi.org/10.1016/j.memsci.2022.121294
603 [43] K. Tiwari, P. Sarkar, S. Modak, H. Singh, S. K. Pramanik, S. Karan, A. Das, Large
604 area self-assembled ultrathin polyimine nanofilms formed at the liquid-liquid interface
605 used for molecular separation, Adv. Mater. 32 (2020) e1905621.
606 http://doi.org/10.1002/adma.201905621
607 [44] N. A. Khan, J. Yuan, H. Wu, T. Huang, X. You, A. U. Rahman, C. S. Azad, M. A.
608 Olson, Z. Jiang, Covalent organic framework nanosheets as reactive fillers to fabricate
609 free-standing polyamide membranes for efficient desalination, ACS Appl. Mater.
610 Interfaces 12 (2020) 27777-27785. http://doi.org/10.1021/acsami.0c06417
611 [45] X. Cheng, Y. Qin, Y. Ye, X. Chen, K. Wang, Y. Zhang, A. Figoli, E. Drioli, Finely
612 tailored pore structure of polyamide nanofiltration membranes for highly-efficient
613 application in water treatment, Chem. Eng. J. 417 (2021) 127976.
614 http://doi.org/10.1016/j.cej.2020.127976
615 [46] Z. L. Qiu, L. F. Fang, Y. J. Shen, W. H. Yu, B. K. Zhu, C. Helix-Nielsen, W. Zhang,
616 Ionic dendrimer based polyamide membranes for ion separation, ACS Nano 15 (2021)
617 7522-7535. http://doi.org/10.1021/acsnano.1c00936
618 [47] Z. Jiang, R. Dong, A. M. Evans, N. Biere, M. A. Ebrahim, S. Li, D. Anselmetti, W.
619 R. Dichtel, A. G. Livingston, Aligned macrocycle pores in ultrathin films for accurate
620 molecular sieving, Nature 609 (2022) 58-64. http://doi.org/10.1038/s41586-022-
621 05032-1
622 [48] W. Lai, L. Liu, J. Bai, L. Xiao, Y. Jiao, Y. Yang, L. Shan, S. Luo, Highly permeable
623 benzene-trisulfonyl chloride-based polysulfonamide membranes fabricated by
624 interfacial polymerization for acid-resistant nanofiltration, Chem. Eng. J. 460 (2023)
625 141708. http://doi.org/10.1016/j.cej.2023.141708

626 [49] Z. Liu, Z. Mi, L. Meng, Y. Huang, D. Zhang, J. Wang, K. Zhang, J. Xiao, P. Liu,
627 Z. Rao, H. He, S. Wang, Quaternary ammonium salts modification preparing charged
628 janus nanofiltration membrane for the simultaneous separation of divalent anions and
629 cations, J. Membr. Sci. 672 (2023) 121440.
630 http://doi.org/10.1016/j.memsci.2023.121440
631 [50] H. Zheng, Z. Mou, Y. J. Lim, B. Liu, R. Wang, W. Zhang, K. Zhou, Incorporating
632 ionic carbon dots in polyamide nanofiltration membranes for high perm-selectivity and
633 antifouling performance, J. Membr. Sci. 672 (2023) 121401.
634 http://doi.org/10.1016/j.memsci.2023.121401
635 [51] H.-L. Zhang, Y.-B. Gao, J.-G. Gai, Guanidinium-functionalized nanofiltration
636 membranes integrating anti-fouling and antimicrobial effects, J. Mater. Chem. A 6
637 (2018) 6442-6454. http://doi.org/10.1039/c8ta00342d
638 [52] Y. Gao, S. Zhao, Z. Qiao, Y. Zhou, B. Song, Z. Wang, J. Wang, Reverse osmosis
639 membranes with guanidine and amine enriched surface for biofouling and organic
640 fouling control, Desalination 430 (2018) 74-85.
641 http://doi.org/10.1016/j.desal.2017.12.055
642 [53] S. Zhang, R. Zhang, R. Li, Z. Zhang, Y. Li, H. Deng, J. Zhao, T. Gu, M. Long, X.
643 Wang, S. Zhang, Z. Jiang, Guanidyl-incorporated nanofiltration membranes toward
644 superior Li^{+}/Mg^{2+} selectivity under weakly alkaline environment, J. Membr. Sci. 663
645 (2022) 121063. http://doi.org/10.1016/j.memsci.2022.121063
646 [54] Z. Hao, X. Tian, V. Mankol, Q. Li, J. Wang, Z. Wang, S. Zhao, Polyamide
647 nanofiltration membrane fabricated with ultra-low concentration triaminoguanidine
648 showing efficient desalination performance, J. Membr. Sci. 672 (2023) 121449.
649 http://doi.org/10.1016/j.memsci.2023.121449
650 [55] X.-H. Ma, Z.-K. Yao, Z. Yang, H. Guo, Z.-L. Xu, C. Y. Tang, M. Elimelech,

651 Nanofoaming of polyamide desalination membranes to tune permeability and
652 selectivity, Environ. Sci. Technol. Lett. 5 (2018) 123-130.
653 http://doi.org/10.1021/acs.estlett.8b00016
654